A theoretical study of the potential energy surface for the reaction OH+CO→CO2+H

Mutsumi Aoyagi and Shigeki Kato

Citation: The Journal of Chemical Physics **88**, 6409 (1988); doi: 10.1063/1.454427
View online: http://dx.doi.org/10.1063/1.454427
View Table of Contents: http://scitation.aip.org/content/aip/journal/jcp/88/10?ver=pdfcov
Published by the AIP Publishing

A theoretical study of the potential energy surface for the reaction $OH + CO \rightarrow CO_2 + H$

Mutsumi Aoyagi[a)]
Department of Chemistry, Faculty of Science, Nagoya University, Chikusa, Nagoya 464, Japan

Shigeki Kato
Department of Chemistry, College of Arts and Sciences, The University of Tokyo, Komaba, Meguro, Tokyo 153, Japan

(Received 22 July 1987; accepted 19 January 1988)

The mechanism of the reaction $OH + CO \rightarrow CO_2 + H$ is studied theoretically. The potential energy surface is constructed by using *ab initio* multiconfiguration (MC) SCF and configuration interaction (CI) calculations. The reaction surface Hamiltonian is derived to estimate the hydrogen tunneling probability. It is found that the first step is the *trans* addition of OH to CO and the *trans–cis* isomerization is the subsequent step to lead the hydrogen elimination from the HOCO. The rate constant is calculated by using the RRKM equation and the curved Arrhenius temperature dependence, experimentally observed, is obtained. We have found here that the effects of both the hydrogen tunneling from the HOCO to products and the backreaction from the HOCO to the reactants are essential to obtain this temperature dependence.

I. INTRODUCTION

In recent years, a number of elementary gas-phase reactions involved in the combustion process have been the subject of extensive research both theoretically and experimentally. The reaction of OH with carbon monoxide:

$$OH + CO \rightarrow CO_2 + H \qquad (1)$$

has generally been considered as the final step for the production of CO_2 in hydrocarbon combustion.[1] In addition, reaction (1) is also known to play an important role in the cycle of converting NO to NO_2 in the atmosphere.[2] Several experimental and kinetic studies of this reaction revealed that reaction (1) has a strongly curved Arrhenius plot; the activation energy at 300 K is nearly equal to zero, but at 2000 K it is about 7 kcal/mol.[3,4]

Smith and Zellner[5] interpreted this in terms of a stable intermediate complex and they proposed that there are almost equal barriers to the dissociation of HOCO to give $OH + CO$ or $CO_2 + H$. Furthermore they suggested that the location of the transition state for the overall reaction is at the barrier leading from HOCO to $CO_2 + H$. They have found that a TST calculation based on these assumptions can reproduce the observed kinetic behavior if the O–C–O angle is collinear at the transition state. Recently, Mozurkewich and Benson[6] have modified RRKM theory considering the backreaction of the intermediate to reactants, and calculated the rate constant and its pressure dependence, where barrier heights of the first and second transition state were chosen in order to fit the experimental data. The results of their calculation predicted that the two barrier heights are nearly equal and that the O–C–O angle is about 160° at the second transition state.

Recently, Radhakrishnan *et al.*[7] studied the reaction of H atom with CO_2 experimentally using the van der Waals complex CO_2HBr. They found that the hot H atoms produced by the 193 nm photolysis of the HBr constituent approaches CO_2 mainly along the direction of the O–C–O axis. OH radical is detected via LIF, and vibrational, rotational, and spin–orbit population distribution were obtained under molecular beam and bulk conditions. The rotational distributions obtained by the molecular beam experiment differ measurably from the experiment under bulk conditions and they interpreted this as direct reaction deriving from short HOCO lifetime and/or interactions between the OH product and the nearby Br which result in deactivation of the OH produced via HOCO decomposition.

Several theoretical works have been reported on the HOCO system. Feller *et al.*[8] performed configuration interaction calculations on the low-lying states of the formyloxyl radical and showed that the potential energy surface of the σ and π states are very different from each other. They have also determined the transition state for fragmentation of HCO_2 to $H + CO_2$ and for rearrangement to HOCO radical by a 1,2-hydrogen shift, but their interest was mainly focused on the potential surface of formyloxyl radical. Recently Mclean and Ellinger[9] determined the structures of the *cis* and *trans* isomers of ground-state HOCO by CI calculations. The *trans* isomer is found to be 3.3 kcal/mol lower in energy than the *cis* one. They have pointed out that electron correlation effects are crucial and the Hartree–Fock approximation did not correctly predict the relative stability of these isomers.

Reaction (1) has also been the subject of theoretical calculation. Harding *et al.*[10] have carried out calculations on the potential surface. They found that the *trans* addition of OH to CO has the lower barrier height and the dissociation of HOCO to $CO_2 + H$ occurs through the *cis* form of the transition state. Schatz *et al*[11] have performed dynamics calculations of $CO_2 + H$ collisions using the potential surface

[a)] Present address: Institute for Molecular Science, Myodaiji, Okazaki 444, Japan.

 0021-9606/88/106409-10$02.10

derived from the *ab initio* calculations by Harding *et al.*

In spite of these experimental and theoretical activities, the mechanism of reaction (1) especially for the origin of negative activation energy has been little understood. More extensive theoretical calculations of the transition state and the reaction intermediate as well as the properties of reaction path would be required for the better understanding of the dynamics of reaction (1). In the present paper, we have carried out multiconfiguration (MC) SCF and CI calculations for the potential energy surfaces of reaction (1). The purpose of this work is to determine the reaction surface in order to discuss the details of the reaction mechanism and to aid in the construction of a global potential energy surface for dynamics calculations.

In Sec. II the calculational methods are described. The result of the calculations are presented for the global feature of potential surface as well as the properties at some critical points on the potential surface. We have also constructed the reaction surface Hamiltonian. In Sec. IV the mechanism of reaction (1) is discussed on the basis of the result of present calculations. The conclusions are also given.

II. METHOD OF CALCULATION

The potential energy surface for reaction (1) was calculated by the unrestricted Hartree-Fock (UHF) and MCSCF method. For the MCSCF wave function, we have chosen the CAS (complete active space) type configurations, where all possible configurations are generated by occupying seven electrons in six orbitals. Six active orbitals [π^2(CO*b*), σ^2(CO*b*), σ^2(OH), σ^1 (radical MO), σ^*(CO*b*), σ^*(OH)] are selected so as to describe the overall reaction process correctly; this includes the formation of the complex and dissociation to products. The total number of configurations in MCSCF wave function is 210 in C_1 symmetry.

The basis set we have used is of double zeta plus polarization (DZP) quality. The Huzinaga–Dunning (9*s*5*p*1*d*/3*s*1*p*)/[4*s*2*p*1*d*/2*s*1*p*] DZP basis set[12] was employed. The exponents for the *d*-polarization function were chosen to be 0.75 and 0.8 for C and O atoms, respectively. The *p*-polarization function with the exponent of 1.0 was employed for H. The geometry optimizations were carried out by using the analytic gradient method. The force constants were obtained by the numerical differentiation of the energy gradient.

In order to obtain more reliable information for the potential surfaces, we have carried out configuration interaction (CI) calculations. The natural orbitals for the MCSCF wave function were used as the one-particle basis functions in the CI calculation. We have constructed CI wave functions which include all single and double electronic excitations from 14 reference configurations. The A_k method[13] was applied to reduce the number of configurations in the CI wave function. The threshold value for the perturbation selection was chosen to be 5 μhartree. An extrapolation was performed. The number of configurations was about 20 000. The multireference Davidson's correction[14] was employed to obtain reasonable estimated values of the full-MRD-CI limit.

We have further carried out the UHF calculations using the triple zeta plus double polarization (TZDP) basis set in order to investigate the effect of the basis set on the features of the potential energy surface. The TZDP basis is the (11*s*6*p*2*d*/6*s*3*p*)/[5*s*3*p*2*d*/3*s*1*p*] basis of Mclean *et al.*[15] augmented by two sets of *d* functions each on C and O atoms. The exponents for the *d*-polarization function were chosen to be 0.5, 1.7 and 0.6, 1.9 for C and O atom, respectively.

We have used the program GAMESS[16] developed by Dupuis *et al.* for the MCSCF calculations and the MRDCI program developed by Buenker[17] for the CI calculations, respectively.

III. POTENTIAL ENERGY SURFACE

A. Global feature of potential energy surface

It has been suggested[5,6] that the reaction (1) proceeds through two subsequent steps. The first step is the formation of the HOCO reaction intermediate through the addition of OH to CO and the second one is the elimination of H from the intermediate HOCO. We have first determined the two saddle point geometries for these steps, denoted SP1 and SP2, as well as the geometry of the HOCO radical.

In Table I, the geometries of these critical points on the

TABLE I. Optimized geometries of critical points on the potential surface.

Species[a]	*r*(CO*a*)	*r*(CO*b*)	∠(OCO)	*r*(OH)	∠(HOC)
trans-SP1	1.128	1.840	122.72	0.980	98.12
	1.129	1.740	122.98	0.954	101.74
cis-SP1	1.131	1.850	123.96	0.983	94.14
	1.132	1.750	123.67	0.956	96.06
trans-HOCO	1.161	1.355	127.97	0.969	107.57
	1.165	1.322	128.40	0.947	110.47
expt.	1.20	1.34	135.0	0.97	105.0
cis-HOCO	1.167	1.342	130.62	0.977	107.07
	1.171	1.312	130.58	0.953	110.05
trans-SP2	1.175	1.258	149.69	1.377	114.37
	1.170	1.203	154.24	1.300	115.95
cis-SP2	1.155	1.226	152.23	1.344	115.52
	1.155	1.203	154.59	1.345	117.17

[a] In each species, values listed in the fist and the second row are MCSCF and UHF optimized geometries, respectively. For the *trans*-HOCO, the experimental value (Ref. 21) is also given.

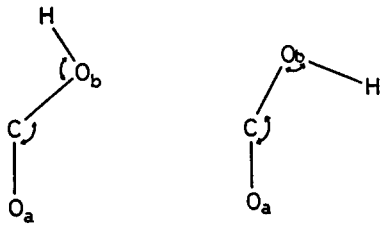

FIG. 1. Structural parameters of *trans* and *cis* HOCO spices.

potential energy surface (saddle points and reaction intermediate) obtained both by the MCSCF and UHF methods are tabulated. The geometrical parameters in Table I are illustrated in Fig. 1. The calculated energies are also summarized in Table II.

We first focused on the heat of reaction for reaction (1). The energy difference between reactants and products was calculated to be 8.1 kcal/mol (1.9 kcal/mol) by the MCSCF method (by UHF). This value is much smaller than the experimental value[18] 25.0 kcal/mol. The CI calculation on the MCSCF orbitals yields 13.2kcal/mol for the heat of reaction, a significant improvement but still much smaller than the experimental value. We further examined the basis set dependence of the heat of reaction; we have used the TZDP basis set in the UHF level calculations. The heat of reaction thus calculated is 2.3 kcal/mol, a slight improvement from the DZP result (1.9 kcal/mol). We performed the CI calculations using the MCSCF orbitals for fragments (OH, CO, CO_2, and an oxygen atom) and obtained the dissociation energies of OH and of CO_2 to CO + O, respectively. These results are summarized in Table III. As seen in Table III, the dissociation energies of OH and CO_2 are also underestimated compared with the experimental values.[19] The error in the CO_2 dissociation energy, 16.8 kcal/mol, is larger than that of OH, 7.8 kcal/mol. This fact indicates that the present calculation significantly underestimates the addition energy of OH to CO (stabilization energy of intermediate) compared with the dissociation energy of H from the HOCO, and therefore the energy of reactant side must be raised by about 9 kcal/mol to obtain more realistic energy relation.

We have found two isomers for the reaction intermediate; the *trans* isomer is more stable then the *cis* one. The present calculation yields 16.9 kcal/mol for the stabilization energy of the *trans* form and 15.5 kcal/mol for the *cis* one. By adding 9.0 kcal/mol mentioned above, these values become 25.9 and 24.5 kcal/mol, respectively. We use these corrected energies for the calculation of the rate constant (see Sec. IV).

For the first saddle point, we found two geometries leading to *trans* and *cis* HOCO. Normal mode analyses at each geometry gave only one normal coordinate with imaginary frequency, implying that these two geometries are true saddle points. The barrier for *trans* addition was calculated to be lower than that of *cis* addition by 6.4 kcal/mol. The effect of electronic correlation is very important in reducing the barrier height for the addition processes. In the *trans* addition, e.g., the barrier height was calculated to be 2.9 kcal/mol at the CI level while the MCSCF and the UHF methods gave 13.5 and 15.4 kcal/mol, respectively.

For the elimination process from the HOCO intermediate, we obtained two saddle points coming directly from the *trans* and *cis* HOCO radical. The energy of *cis* elimination is lower than *trans* elimination by 19.6 kcal/mol. The barrier height for the *cis* elimination was calculated to be 35.3 kcal/mol at the CI level. It is noteworthy that the UHF calculations with the TZDP basis set reduce the barrier height by only 1.3 kcal/mol compared with the DZP-UHF result.

The results are summarized in Fig. 2. As seen in the figure, reaction (1) proceeds as follows. The first step is the *trans* addition of OH to CO. The *trans–cis* isomerization is a subsequent step which leads to H elimination from HOCO. The calculated barrier height for this isomerization process was rather low, 9.3 kcal/mol for UHF, 7.3 kcal/mol for MCSCF, respectively. Thus *trans–cis* isomerization is facile, the energy supplied by the addition process being well above the barrier. The final step, hydrogen elimination from the HOCO, seems to mainly occur by tunneling because the energy of SP2 is higher than the energy of the reactant pair. The result discussed here is consistent with the previous experimental[5,6] and theoretical[10] evidence for this reaction. Details of the reaction process will be discussed in subsequent sections.

B. Addition of OH to CO

As shown above, the transition state for the addition process is a loose transition state. To obtain more detailed information on the transition state structure, we have carried out geometry optimizations at the *trans* form with the

TABLE II. Total energies (in hartree) and relative energies (in kcal/mol) for critical points obtained by UHF, MCSCF, and MRD-CI calculations with DZP basis set.

Species	UHF	MCSCF	MRD-CI
OH + CO	− 188.168 74(5.5)	− 188.215 30(4.5)	− 188.606 42(16.9)
trans-SP1	− 188.144 13(20.9)	− 188.193 83(18.0)	− 188.601 79(19.8)
cis-SP1	− 188.134 07(27.3)	− 188.186 50(22.6)	− 188.593 20(25.2)
trans-HOCO	− 188.177 50(0.0)	− 188.22 246(0.0)	− 188.633 35(0.0)
cis-HOCO	− 188.177 05(0.3)	− 188.222 28(0.1)	− 188.631 07(1.4)
trans-SP2	− 188.072 18(66.1)	− 188.130 66(57.6)	− 188.545 93(54.9)
cis-SP2	− 188.106 28(44.7)	− 188.165 57(35.7)	− 188.577 12(35.3)
CO_2 + H	− 188.171 74(3.6)	− 188.228 15(− 3.6)	− 188.627 41(3.7)

[a] In the parentheses, energies relative to *trans*-HOCO are given.

TABLE III. Total energies (in hartree) and dissociation energies (in kcal/mol) of OH and CO_2 obtained from the UHF, MCSCF, and MRD-CI calculations.

	UHF	MCSCF	MRD-CI
OH	−75.410 21	−75.429 27	−75.561 37
O+H	−75.303 37	−75.298 23	−75.408 33
$D_e\cdot$(OH)	67.1	82.2	96.0 (103.8)
CO_2	−187.674 10	−187.730 68	−188.129 77
CO+O	−187.564 25	−187.592 85	−187.955 75
$D_e\cdot(CO_2)$	68.9	86.5	109.2 (126.0)

[a] $D_e\cdot$ denotes the dissociation energy for OH and CO_2. In the parentheses, experimental values (Ref. 19) are given.

O*b*–C distance fixed. Thus we obtain the potential energy surface near the transition state in the form

$$V(R,\{q\}) = W(R) + \frac{1}{2}\sum_{ij} f_{ij}(R)\Delta q_i \Delta q_j$$

$$\Delta q_i = q_i - q_i^0(R), \tag{2}$$

where $W(R)$ is the potential energy along the O*b*–C distance and f_{ij}'s are the harmonic force constants for the remaining five internal coordinates q_i and q_j, respectively. The geometry optimization and the force constant were obtained with the UHF/DZP wave function. The potential energy $W(R)$ was calculated by the MCSCF-CI procedure at the UHF optimized geometry.

The O*b*–C distance of saddle point (*trans*-SP1) was shifted to 1.879 Å. Other geometrical parameters are $r(\mathrm{CO}a) = 1.123$, $\angle(\mathrm{OCO}) = 121.47$, $r(\mathrm{OH}) = 0.955$, $\angle(\mathrm{HOC}) = 100.35$ and the barrier height is 4.8 kcal/mol. Using the potential function given in Eq. (2), the Hamiltonian can be written in the following form with the adiabatic approximation for the five vibrational degrees of freedom (see Appendix A):

$$H = \frac{1}{2}P_R S P_R + \frac{1}{2}J_0 I_0 J_0 + W(R) + \sum_{k=1}^{5} \hbar\omega_k(R)\left(n_K + \frac{1}{2}\right). \tag{3}$$

The frequencies $\omega(R)$ were obtained by the conventional GF matrix method. The diagonal force constants were reduced by multiplying by a factor of 0.8 to reproduce the experimental fundamental frequencies of the HOCO radical.

We have applied the variational transition state theory[20] and obtained the transition state geometry as well as the reaction rate for the addition process. The temperature we used was 300 K. The calculated rate constant was 1.1×10^{-12} cm^3 molecule^{-1} s^{-1} at the transition state geometry, $r(\mathrm{CO}a) = 1.121$, $\angle(\mathrm{OCO}) = 123.56$, $r(\mathrm{CO}b) = 1.861$, $r(\mathrm{OH}) = 0.954$, and $\angle(\mathrm{HOC}) = 102.75$.

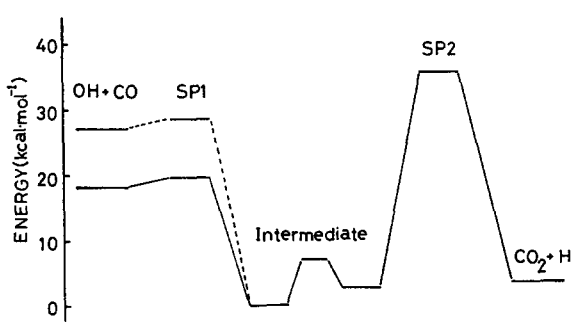

FIG. 2. Schematic diagram of OH + CO potential energy surface. The potential energy for the reactant side is corrected by shifting about 9 kcal/mol from the calculated value, as shown with the dashed lines.

C. Reaction intermediate

There are several experimental and theoretical studies on the properties of the HOCO radical. Although there is no experimental evidence for the relative stability of *trans*- and *cis*-HOCO, Mclean and Ellinger,[9] and Feller *et al.*[8] made *ab initio* calculations on both isomers of HOCO. Mclean and Ellinger made various levels of calculations and proposed that the *trans* isomer is more stable than the *cis* one by 3.3 kcal/mol at their best estimated value. On the other hand, Feller *et al.* obtained a different result. Our present calculations showed that the *trans* isomer is more stable than the *cis* one by 1.1 kcal/mol at the CI level. Milligan and Jacox[21] observed the infrared spectra of the HOCO radical in the CO matrix. The results of a normal mode analysis of our energies are tabulated in Table IV both for the *trans* and *cis* forms. MCSCF and UHF methods gave comparable results. The calculated results are consistent with the experimental results in the ordering of the normal vibrations, but the harmonic frequencies are systematically overestimated by 10%–15%. The overestimation of the calculated frequencies is a common trend of this level of calculations.[22] To obtain more realistic frequencies, the diagonal element of the force constant matrix were reduced by multiplying by a factor of 0.8. With this the largest discrepancy between the experimental and theoretical values was 7 %. The barrier height of *trans–cis* isomerization was calculated to be 7.0 kcal/mol at the CI level. This value is comparable with the calculations of Ref. 9. Therefore, we can expect that equilibrium between the *trans* and *cis* conformers is readily achieved under the experimental conditions.

TABLE IV. Vibrational frequencies (cm^{-1}).

Species	(A) Critical points on the potential surface *trans*-SP1	*cis*-SP1	*trans*-HOCO	*cis*-HOCO	*trans*-SP2	*cis*-SP2
O-H str.	3639	3589	3778(3456)[a]	3646(3316)	2687i	2610i
C-Oa str.	2267	2227	2094(1833)	2044(1797)	2342	2231
H-O-C bent	965	999	1312(1261)	1362(1261)	1056	1051
C-Ob str.	584i	647i	1081(1077)	1095(1088)	1582	1550
O-C-O bent	360	320	650(615)	632(620)	687	646
torsion	256	52	405(--)	611(--)	523	613

Method	(B) *Trans*-HOCO obtained by UHF and MCSCF methods MCSCF	UHF	UHF scaled	Expt.[b]
O-H str.	3778	4144	3706	3456
C-Oa str.	2094	2097	1861	1833
H-O-C bent	1312	1368	1205	1261
C-Ob str.	1081	1200	1077	1077
O-C-O bent	650	682	606	615
torsion	405	536	479	--

[a] The experimental values (Ref. 21) are shown in parentheses.
[b] Reference 21.

D. Hydrogen elimination from HOCO intermediate

As discussed above, the *cis* saddle point is lower in energy than the *trans* saddle point. To describe this elimination process, we have chosen two internal coordinates, the O*b*–H distance and the O–C–O angle, denoted r_1 and r_2, as the large amplitude coordinates. Thus the potential energy surface can be written as

$$V(r_1,r_2,\{q\}) = W(r_1,r_2) + \frac{1}{2}\sum_{ij} f_{ij}(r_1,r_2)\Delta q_i \Delta q_j$$

$$\Delta q_i = q_i - q_i^0(r_1,r_2), \qquad (4)$$

where $W(r_1,r_2)$ is the two-dimensional potential energy surface as a function of r_1 and r_2 and the f_{ij}'s are the elements of the force constant matrix for the remaining coordinates q_i's. We have carried out the geometry optimization with the UHF wave function at 16 points for the (r_1,r_2) pair. The two-dimensional surface was recalculated by the MCSCF-CI procedure. A contour plot of the potential energy surface is shown in Fig. 3. The new saddle point is located at r(C–O*a*) = 1.155, r(C–O*b*) = 1.188, ∠(O–C–O) = 153.86, r(O–H) = 1.421, and ∠(H–O–C) = 118.64 with a barrier height of 36.5 kcal/mol. The diagonal elements of force constant matrix were scaled with the same factor as in the SP1 and HOCO intermediate.

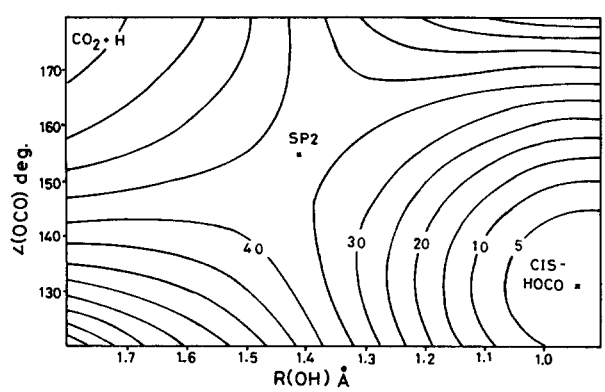

FIG. 3. Potential energy contour map for the region of H elimination process. Two internal coordinates C–O*b* distance and O–C–O angle, denoted r_1 and r_2, are chosen as the large amplitude coordinates. The other internal coordinates are optimized with the UHF gradient method and the potential surface is recalculated by the MCSCF-CI procedure. The relative energy (in kcal/mol) to *cis*-HOCO and the region of the critical point are also shown.

The potential energy $W(r_1,r_2)$, force constant matrix, and the origin of internal coordinate $q_i^0(r_1,r_2)$ were expressed by the analytic functions (see Appendix B). These analytic functions were fitted to reproduce the values at the *cis* intermediate and product pair.

In Fig. 4, the harmonic frequencies for the normal coordinates are plotted. The frequencies for the stretching and the bending modes are smoothly changing as a function of r_1 and r_2. Although the torsional frequency changes only a little in almost the whole region of r_1 and r_2 pairs, it rapidly increases as the O–C–O angle is open to linear. With the potential function given in Eq. (4), we can use the reaction surface Hamiltonian model developed by Carrington and Miller[23] to describe the dynamics of chemical reaction. The Hamiltonian can be represented in the zeroth order vibrational adiabatic approximation (see Appendix A)

$$H = \frac{1}{2}P_r S^t P_r + \frac{1}{2}J_0 I_0^t J_0 + W(r_1,r_2) + \sum_{k=1}^{3N-8} \hbar\omega_k(r_1,r_2)\left(n_k + \frac{1}{2}\right) (t\text{:transpose}). \qquad (5)$$

Since the barrier height for the *cis*-elimination process is higher than energy of reactant pair, the tunneling effect is important in describing the reaction process. In order to estimate the tunneling probability, we have calculated the intrinsic reaction coordinate (IRC)[24] in the two-dimensional coordinate space (r_1,r_2). The IRC was obtained from the following simultaneous differential equation with the effective potential surface where the four vibrational motions are in their zero-point energy level:

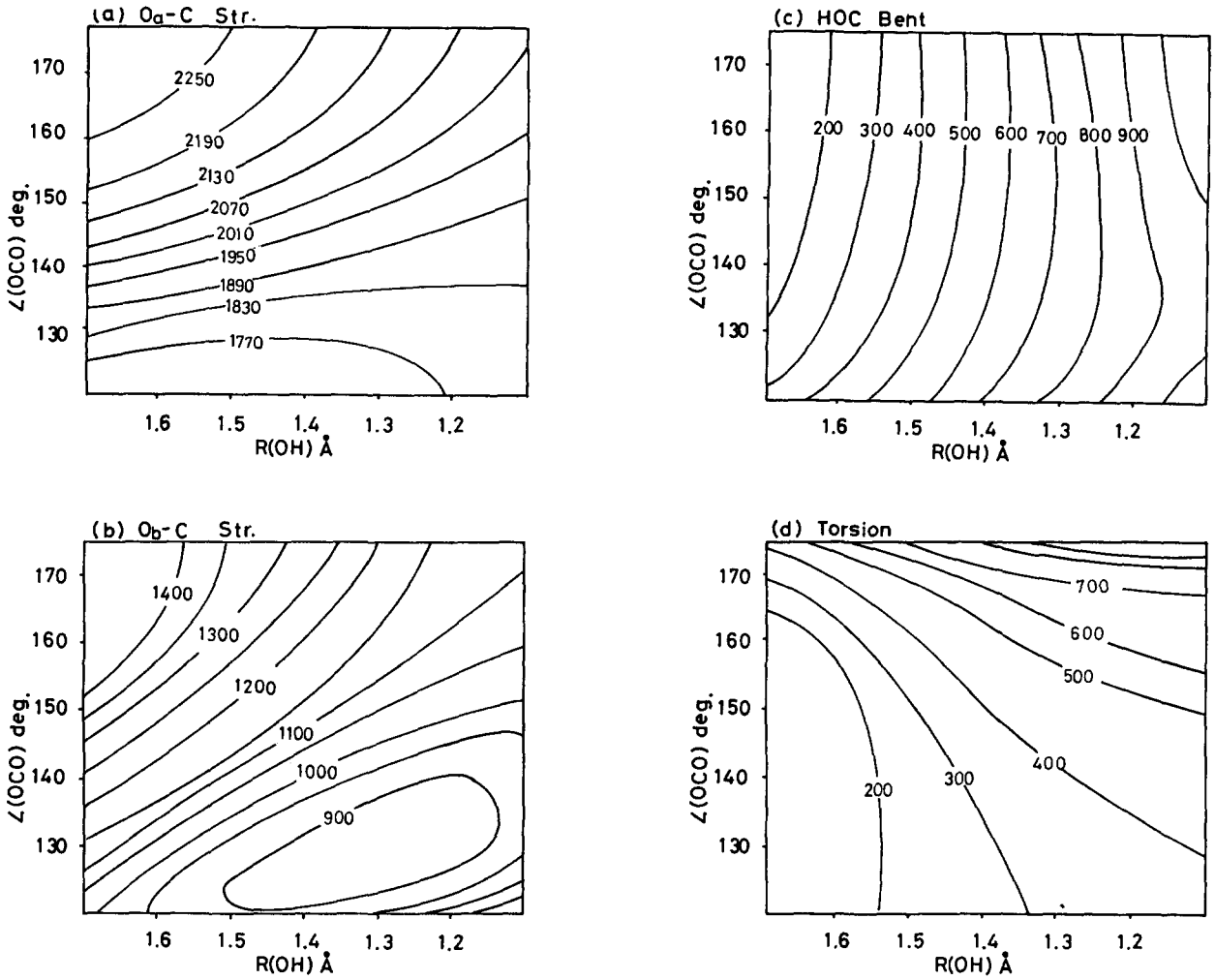

FIG. 4. Contour maps for the harmonic frequencies obtained by using the UHF wave function. Frequency maps for O*a*–C, O*b*–C stretching, H–O–C bending and torsional modes are shown in (a)–(d), respectively. The unit of frequency is cm^{-1}.

$$\frac{dr_n}{ds} = \frac{dW}{ds}\sum_j g_{jn}\frac{\partial W}{\partial r_j} \quad (n = 1,2),$$
$$\frac{dW}{ds} = -\left[\sum_{ij}\frac{\partial W}{\partial r_i}\frac{\partial W}{\partial r_j}g_{ij}\right]^{-1/2}, \tag{6}$$

where g_{ij} is the G matrix element for r_i and r_j.

The reaction coordinate is described by the O–C–O bending coordinate near the intermediate and becomes the OH stretching mode upon approaching the saddle point. The energy levels of vibrational modes perpendicular to the reaction coordinate were obtained by using the harmonic oscillator approximation. The resultant effective potential energy curve and IRC are shown in Fig. 5. The tunneling probability was calculated by the WKB approximation for the vibrational ground state and the result was $P = 0.01$ for $E = 25.0$ kcal/mol where E is the energy in the reaction coordinate and is measured relative to the *cis*-HOCO. Although the tunneling probability obtained here is very approximate, it seems that the effect of tunneling is very important when the energy is near that of the saddle point. We will carry out more realistic calculations for the dynamics in future work.

IV. DISCUSSION AND CONCLUSION

We have studied the potential energy surface of reaction (1) using *ab initio* UHF and MCSCF-CI methods. First we discussed the geometries of critical points and the features of

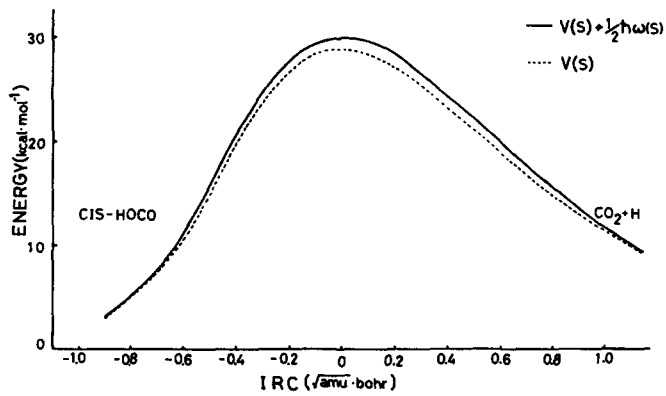

FIG. 5. The potential energy curve (---) along the intrinsic reaction coordinate and the effective potential curve (–) for hydrogen tunneling.

the potential energy surface. Next we considered the reaction mechanism based on the results of the present calculations.

For the addition of OH to CO, we have determined the potential energy curve along the reaction coordinate. The structure of the transition state and the rate constant were obtained by using variational transition state theory. Mozurkewich *et al.*[6] have proposed two models for the first transition state geometry. One was a very loose transition state where the O*b*–C distance was taken to be the van der Waals distance (2.8 Å), the other was comparatively tight and OH torsion was assumed to be a free internal rotation. Our result obtained from the present VTST calculation corresponds to their latter model; the calculated O*b*–C distance (1.861 Å) is a little longer than that of Benson's model (1.7 Å).

The structure of the intermediates and the harmonic frequencies were obtained by UHF and MCSCF methods. The HOCO intermediate has been observed in matrix isolation studies,[21] and its IR spectrum has been assigned. The experimentally assumed structure is given in Table I with the theoretical values. Mclean and Ellinger[9] have also determined the geometries of HOCO using a series of the CI calculations. The results of their best estimated values are $r(\mathrm{CO}a) = 1.167$, $r(\mathrm{CO}b) = 1.330$, $\angle(\mathrm{OCO}) = 126.0$, $r(\mathrm{OH}) = 0.957$, and $\angle(\mathrm{HOC}) = 108.0$ for the *trans* isomer. Our present results are in good agreement with experimental and theoretical values. As seen in the Table I, the O*b*–C and O*a*–C distances of the intermediate complex suggest that the radical center moves to the carbon atom from the oxygen atom as reaction proceeds along the reaction path and forms the intermediate. The stabilization energy of the intermediate (*trans* form) was calculated to be 16.9 kcal/mol relative to reactants at the CI level. Considering the calculated energy error (about 9 kcal/mol) of the reactant energy, we expect that the intermediate is stabilized in energy at about 26 kcal/mol. This result is still smaller than the value proposed by Mozurkewich *et al.*[6]

For the hydrogen elimination process from the HOCO intermediate, several groups have proposed transition state structures. The structure assumed by Smith and Zellner[5] was that with the heavy atoms linear. Golden[25] proposed a completely linear transition state. Finally Mozurkewich *et al.*[6] chose a bent geometry where the O–C–O bending angle is 160°. Our result supports that of Mozurkewich *et al.*

Reaction (1) is considered to occur by the following reaction scheme:

$$\begin{array}{l} \mathrm{OH} + \mathrm{CO} \underset{k_{-1}}{\overset{k_1}{\rightleftarrows}} \textit{trans}\text{-HOCO} \\ \qquad\qquad\quad k_2 \downarrow \uparrow k_{-2} \quad k_3 \\ \qquad\quad \textit{cis}\text{-HOCO} \rightarrow \mathrm{CO_2} + \mathrm{H}. \end{array} \tag{7}$$

If we apply the steady state assumption to the population of the *cis* and *trans* reaction intermediates, the overall rate constant can be expressed by

$$K(E) = \frac{k_1 k_3}{\dfrac{k_{-1}k_{-2}}{k_2} + \left(\dfrac{k_{-1}}{k_2} + 1\right)k_3}. \tag{8}$$

Since the barrier height of *cis–trans* isomerization in the intermediates is much lower than that of the decomposition reaction, HOCO(*trans*) → HO + CO, we can assume that the term k_{-1}/k_2 is nearly equal to zero. The ratio of rate constants k_{-2}/k_2 is replaced by the equilibrium rate con-

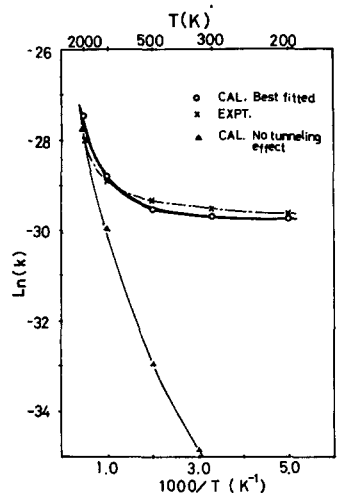

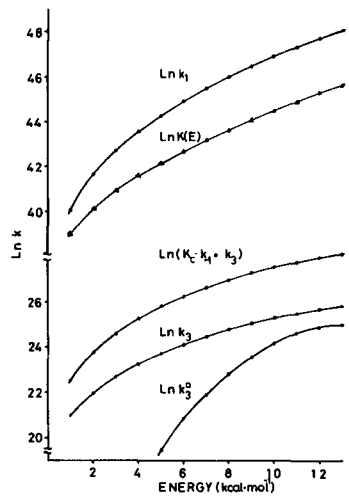

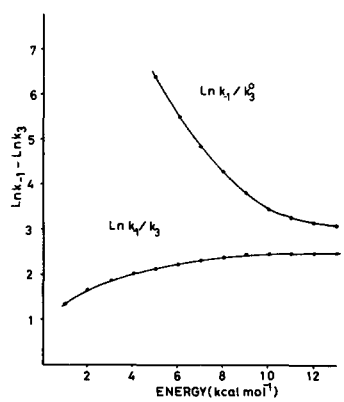

FIG. 6. (a) Arrhenius plots of the caluculated rate constants and the experimental rate constant for the reaction (1). (b) Microcanonical rate constants for the reaction (1). k_1, k_{-1}, and k_3 are defined in Eq. (7). k_3^0 denotes the rate of the H-elimination process without tunneling. The energy zero is set at the top of SP1. (c) The rate constant of the backward reaction, HOCO → reactant, relative to the H-elimination rate.

stant K_c between the two isomers. The rate constant is thus written in the form

$$\ln K(E) = \ln k_{-1} + \ln k_3 - \ln(k_c k_{-1} + k_3). \quad (9)$$

With the use of the potential surface properties obtained in the present work, we have calculated the microcanonical rate constant $K(E)$ as a function of the total energy of the system. The rate constant of the initial addition reaction k_1 and its reverse reaction k_{-1} were calculated by microcanonical variational transition state theory.[20] Since tunneling is important for the hydrogen elimination reaction from *cis*-HOCO, we included the tunneling probability in estimating the rate constant k_3. Finally we have carried out Boltzman averaging of $K(E)$ to the energy of the reactant pair.

The results are shown in Figs. 6(a)–6(c). As seen in Fig. 6(a), the calculated overall rate constant is underestimated compared with the experimental value.[3,26,27] To achieve better agreement with the experimental rate constants, we have made the following corrections on the potential energy surface: (1) we first raised the energy of the reactant pair by 0.6 kcal/mol to reproduce the experimental heat of reaction. (2) We further shifted the energies of saddle points SP1 and SP2. We have obtained the best fit curve shown in Fig. 6(a), to the experimental result with the barrier heights 1.3 and 5.6 kcal/mol, of SP1 and SP2, respectively. We also calculated the rate constant without including the tunneling effect for the corrected potential surface and obtained the curve far from the experimental result, seen also in Fig. 6.

In order to investigate the origin of the curved Arrhenius plot, we have plotted the energy dependence of each term in Eq. (9). As shown in Fig. 6(b), in a low energy region, curvature of $\ln k_1$ is almost the same as that of $\ln(K_c k_1 + k_3)$. So the total $\ln K(E)$ curve is largely affected by $\ln k_3$. On the other hand, in higher energy, the $\ln K(E)$ curve is parallel to the k_1. Further, as seen in Fig. 6(c), $\ln k_1 - \ln k_3$ increases monotonously, as the energy is higher. It is found that the rate constant of the backreaction from the HOCO to reactants increases more rapidly with total energy than that of the hydrogen elimination process. This is due to the fact that the barrier height of the second transition state is higher in energy than that of the first and due to the fact that the hydrogen elimination process mainly occurs by tunneling, which is slow compared with the normal process.

Mozurkewich *et al.* have employed almost the same barrier heights for the first and second transition states (i.e., $V_{SP1} = V_{SP2} = 1.0$ kcal/mol). To obtain the curved Arrhenius plot, they emphasize the the importance of the backreaction and the difference of the bonding character between the two transition states. The present calculation of the potential energy surface and the rate constant, however, shows that the V_{SP2} is about 4.3 kcal/mol higher in energy than V_{SP1}. Therefore, the origin of the curved Arrhenius plot and the negative activation energy should be reinterpreted as the competitive behavior between the backreaction from intermediates to reactants and the hydrogen elimination process including the effect of tunneling.

Paraskevopoulos and Irwin[28] have measured the rate constant for OD + CO at 300 K. They find that this rate constant is about one-third of that for OH + CO. This indicates that the effect of hydrogen tunneling is very important at low temperature considering the large difference of rate constant between OH and OD reactions.

The results obtained from the present calculations can be summarized as follows:

(1) The first step of reaction (1) is the *trans* addition of OH to CO. The transition state for this addition process is a loose one.

(2) The second step is the *trans–cis* isomerization which leads to the final step of the hydrogen elimination from the HOCO intermediate.

(3) The energy difference between the first and the second transition state is calculated to be 6.5 kcal/mol and is estimated to be 4.3 kcal/mol using the result of the rate constant calculation. The final step, hydrogen elimination from HOCO, seems to mainly occur by the tunneling process because the energy of SP2 is higher than that of reactant pair.

(4) The origin of the curved Arrhenius plot is interpreted as the results of competitive behavior between the backreaction from intermediates to reactants and the hydrogen elimination process including the effect of tunneling.

ACKNOWLEDGMENTS

The authors are grateful to Professor K. Hirao and Professor K. Takatsuka for their valuable discussions. Numerical calculations were carried out at IMS Computer Center and Nagoya University Computer Center.

APPENDIX A

The reaction surface Hamiltonian has been derived in almost the same way as that of Carrington and Miller.[23] The definition of small amplitude vibrational coordinates (SAC's) is, however, slightly different. In Ref. 23, the SACs are taken to be orthogonal to the tangent plane of the reaction surface $a(r_1, r_2)$ in the mass-weighted Cartesian coordinate space

$$\sum_{i=1}^{N} \frac{\partial a_i}{\partial r_n} \cdot \frac{\partial a_i}{\partial Q_K} = 0 \quad (n = 1,2;\ k = 1,2,...,3N-8), \quad (A1)$$

where r_1 and r_2 are the large amplitude coordinates (LACs) and Q_k is the kth SAC, respectively. The vector $a_i(r_1, r_2)$ represents the position of ith atom in the mass-weighted Cartesian coordinate representation and

$$a(r_1, r_2) = \{a_1, a_2, ..., a_N\}, \quad (A2)$$

where N is the number of atoms. In the present, we have defined the SACs so as to satisfy the relation

$$\frac{\partial V}{\partial Q_k} = \sum_{i=1}^{N} \frac{\partial V}{\partial a_i} \cdot \frac{\partial a_i}{\partial Q_k} = \sum_{n=1}^{2} \frac{\partial V}{\partial r_n} \sum_{i=1}^{N} \frac{\partial r_n}{\partial a_i} \cdot \frac{\partial a_i}{\partial Q_k} = 0. \quad (A3)$$

This means that the SACs are linearly independent of the LACs, r_1 and r_2, and not necessarily normal to the reaction surface. The SACs in the present work, Q_k, are obtained by performing the normal mode analyses for the harmonic term in Eq. (4) as the function of r_1 and r_2.

The resultant kinetic energy term is given in the same form as in Ref. 23:

TABLE V. Fitted parameters.

	(A) Internal coordinates						
	f_1	f_2	C_1	C_2	C_3	C_4	C_5
$R(CO_a)$	2.2129[a]	2.1656	0.7849	−0.3566	0.3907	−1.6873	0.9967
$R(CO_b)$	2.4793	2.1656	0.9497	−0.1144	0.5398	−1.5532	0.6680
∠(HOC)	1.9207	3.1416	−0.0215	−0.2132	0.1399	−0.2423	0.3300
	(B) Force constants						
Diagonal	f_1	f_2	C_1	C_2	C_3	C_4	C_5
CO_a	1.1110[a]	1.2469	1.7152	0.5898	−0.1225	−2.8386	0.5199
CO_b	0.5039	1.2469	0.2902	−0.2237	0.5455	−1.2044	1.1406
HOC	0.1859	0.0	0.3477	0.3467	0.6038	−0.6298	−0.3333
torsion	0.0264	0.0	−0.5674	−0.8799	1.2349	−1.5424	2.1338
Off-diagonal	f_1	f_2	C_1	C_2	C_3	C_4	C_5
CO_a–CO_b	0.1110	0.1387	1.4502	1.5990	0.5188	−0.2073	0.9445
CO_a–HOC	0.0053	0.0	3.0230	1.0764	−0.9293	−4.8476	−0.1061
CO_b–HOC	0.0436	0.0	1.3378	−0.2663	0.1683	−0.6381	0.1073

[a] Values in the table are all in atomic units.

$$T=\frac{1}{2}\sum_{k=1}^{3N-8}P_k^2+T'$$

and

$$T'=\tfrac{1}{2}(J-\pi)\cdot(I_0+b)^{-1}I_0'(I_0+b)^{-1}\cdot(J-\pi). \tag{A4}$$

For the notations of Eq. (A4), see Ref. 23.

In the present Hamiltonian, the additional terms

$$U_k^n=\sum_{i=1}^{N}\frac{\partial a_i}{\partial r_n}\cdot L_{ik}\quad(n=1,2;\ k=1,2,\ldots,3N-8) \tag{A5}$$

are included because the coordinate systems used here do not satisfy the condition (A1). The original Carrington–Miller's Hamiltonian is modified as follows:

(1) The coupling elements in the vibrational angular momentum vector π is replaced by

$$B_{k,k'}^{(n)}=U_k^n+\sum_{i=1}^{N}\frac{\partial L_{ik}}{\partial r_n}\cdot L_{ik'}. \tag{A6}$$

(2) The elements of inertia tensor I_0 are replaced by

$$S_{n,n'}=\sum_{i=1}^{N}\frac{\partial a_i}{\partial r_n}\cdot\frac{\partial a_i}{\partial r_{n'}}-\sum_{k=1}^{3N-8}U_k^nU_k^{n'}. \tag{A7}$$

(3) The elements of linear correction tensor b:

$$b=\sum_{k=1}^{3N-8}b_kQ_k, \tag{A8}$$

are given by

$$b_k=\begin{pmatrix} b_k^{(n,n')}b_k^{(n)} \\ b_k'^{(n)}\,b_k^{(0)}\end{pmatrix}, \tag{A9}$$

where

$$b_k^{(n,n')}=\sum_{i=1}^{N}\left[\frac{\partial a_i}{\partial r_n}\cdot\frac{\partial L_{ik}}{\partial r_{n'}}+\frac{\partial a_i}{\partial r_n}\cdot\frac{\partial L_{ik}}{\partial r_n}+\sum_{l=1}^{3N-8}\left(U_l^nL_{il}\cdot\frac{\partial L_{ik}}{\partial r_{n'}}+U_l^{n'}\cdot\frac{\partial L_{ik}}{\partial r_n}\right)\right] \tag{A10}$$

and

$$b_k'^{(n)}={}'b_k^{(n)}+\sum_{l=1}^{3N-8}U_l^n\left[\sum_{i=1}^{N}L_{i,l}\times L_{i,k}\right]. \tag{A11}$$

It is apparent that the present Hamiltonian becomes the same as that of Carrington and Miller if we neglect the terms U_k^n. The final form of the reaction surface Hamiltonian is obtained by expanding a matrix $(I+b)^{-1}$ to the zeroth order in b and by applying a usual vibrational adiabatic approximation to the $3N-8$ vibrational degrees of freedom

$$H=\frac{1}{2}P_rS'P_r+\frac{1}{2}J_0I_0'J_0+W(r_1,r_2)+\sum_{k=1}^{3N-8}\hbar\omega_k(r_1,r_2)\left(n_k+\frac{1}{2}\right). \tag{A12}$$

As seen in Eq. (31), one internal coordinate can also be chosen as LAC. The Hamiltonian is derived in the same way.

APPENDIX B

The potential energy function $W(r_1,r_2)$ was obtained by using the two-dimensional spline fitting procedure. The energies at the *cis*-SP2 region were obtained by MCSCF-MRDCI calculations. Those on the *cis*-HOCO region were estimated by the calculated force constants and MCSCF-MRDCI energy of the *cis*-HOCO. The total sampling point used for the spline fitting are 36 points.

The analytic form of the origin of the internal coordinates and the force constants were written by

$$f(r_1,r_2)=f_1[1-\tanh g(r_1,r_2)]+f_2\tanh g(r_1,r_2), \tag{B1}$$

where f_1 and f_2 are values of the *cis*-HOCO and the products CO_2+H, respectively. $g(r_1,r_2)$ is given by

$$g(r_1,r_2)=C_1(r_2-r_2^0)+C_2[(r_1-\pi)^2-(r_1^0-\pi)^2]+C_3(r_2-r_2^0)^2+C_4(r_2-r_2^0)(r_1-\pi)^2+C_5(r_1-\pi)^2[(r_1-\pi)2-(r_1^0-\pi)^2], \tag{B2}$$

where r_1^0 and r_2^0 are the O–C–O angle and the OH distance of the *cis*-HOCO, $r_1^0 = 2.2791$ rad and $r_2^0 = 1.8010$ bohr. The parameters C_1–C_5 were determined by the least square fitting procedure using the optimized geometries and the force constants calculated by the UHF method. They are listed in Table V(A) and V(B), respectively.

[1]B. Lewis and G. Elbe, *Combustion Flames and Explosion of Gases* (Academic New York, 1961), p. 90.
[2]R. S. Berry, Annu. Rev. Phys. Chem. **22**, 47(1971).
[3]D. L. Baulch and D. D. Drysdale, Combust. Flame. **23**, 215 (1974).
[4]I. W. Smith, Chem. Phys. Lett. **49**, 112 (1977).
[5]I. W. Smith and R. Zellner, J. Chem. Soc. Faraday Trans. 2 **69**, 1617 (1973).
[6]M. Mozurkewich and S. W. Benson, J. Phys.Chem. **88**, 6429 (1984); M. Mozurkewich, J. J. Lamb, and S. W. Benson, *ibid.* **88**, 6435 (1984).
[7]G. Radhakrishnan, S. Buelow, and C. Wittig, J. Chem.Phys. **84**, 727 (1986).
[8]D. Feller, E. S. Huyser, W. T. Borden, and E. R. Davidson, J. Am. Chem. Soc. **105**, 1459 (1983).
[9]A. D. Mclean and Y. Ellinger, Chem. Phys. **94**, 25 (1985).
[10]L. B. Harding, Argonne National Laboratory, Annual Report, 1982–1983, p. 3. It should be noted that Harding *et al.* found neither a *cis* saddle point for OH + CO addition step nor a *trans* saddle point for the H elimination from the HOCO by using SD-CI method. We here obtained these saddle points by using the MCSCF method. The more elaborated calculation must be performed to determine the existence of these saddle points. These saddle points are, however, not involved in the present reaction and do not affect the rate constant value calculated in the next section.
[11]G. Schatz, 3rd Symposium on Theoretical Chemistry, Tokyo, Japan, August 1986.
[12]S. Huzinaga, J. Chem. Phys. **42**, 1293 (1965); T. H. Dunning, *ibid.* **53**, 2823 (1970).
[13]Z. Gershgorn and I. Shavitt, Int. J. Quantum Chem. **2**, 751 (1968).
[14]E. R. Davidson, in *World of Quantum Chemistry*, edited by R. Daudel and B. Pullman (Dordrecht, Netherlands, 1974).
[15]A. D. Mclean, G. H. Loew, and D. S. Berkowitz, J. Mol. Spectrosc. **64**, 184 (1977).
[16]M. Dupuis, D. Spangler, and J. Wendoloski, NRCC Software Catalog, Vol. 1, 1980, Program GG01 (GAMESS).
[17](a) R. J. Buenker, in *Proceeding of Workshop on Quantum Chemistry and Molecular Physics*, Wollongong, Australia, 1980; (b) R. J. Buenker and R. A. Phillips, J. Mol. Struct. **123**, 291 (1985).
[18]R. M. Fristrom and A. A. Westenberg, *Flame Structure* (McGraw–Hill, New York, 1965), p. 355.
[19]*JANAF Termochemical Tables*, Natl. Bur. Ser. Natl. Bur. Stand. (U.S. GPO, Washington, D.C. 1971).
[20]B. C. Garrett and D. G. Truhlar, J. Chem. Phys. **70**, 1593 (1979).
[21]D. E. Milligan and M. E. Jacox, J. Chem. Phys. **54**, 927 (1971).
[22]P. Pulay, in *Modern Theoretical Chemistry*, edited by H. F. Schaefer III (Plenum, New York, 1977), Vol. 4, p. 153.
[23]T. J. Carrington and W. H. Miller, J. Chem. Phys. **81**, 3942 (1984).
[24]K. Fukui, S. Kato, and H. Fujimoto, J. Am. Chem. Soc. **97**, 1 (1975); S. Kato and K. Fukui, *ibid.* **98**, 6395 (1976).
[25]D. M. Golden, J. Phys. Chem. **83**, 108 (1979).
[26]D. D. Davis, S. Fischer, and R. Schiff, J. Chem. Phys. **61**, 2213 (1974).
[27]A. R. Ravishankara and R. L. Thompson, Chem. Phys. Lett. **99**, 377 (1983).
[28]G. Paraskevopoulos and R. S. Irwin, Chem. Phys. Lett. **93**, 138 (1982).